ACS Catalysis

RESEARCH ARTICLE

pubs.acs.org/acscatalysis

Predictive Model for the Design of Plasmonic Metal/Semiconductor Composite Photocatalysts

David B. Ingram, Phillip Christopher, Jonathan L. Bauer, and Suljo Linic*

Department of Chemical Engineering, University of Michigan, Ann Arbor, Michigan 48109, United States

ABSTRACT: We demonstrate the design of composite plasmonic metal/semiconductor photocatalysts, which show enhanced visible light photocatalytic activity compared to the semiconductor alone. We show that the overlap between the illumination source spectrum, semiconductor absorbance spectrum and metal nanoparticle surface plasmon resonance spectrum provides a useful descriptor for predicting the relative rate enhancements induced by metal surface plasmons for composite photocatalysts with similar arrangements of metal and semiconductor building blocks. We also show that optical simulations can be used to predict the value of the descriptor of photocatalytic activity for any arbitrary combination of illumination source, semiconductor, and plasmonic metal, and therefore guide the formulation of optimal composite photocatalysts. We have used optical simulations to identify optimal plasmonic nanostructures for a few model semiconductors.

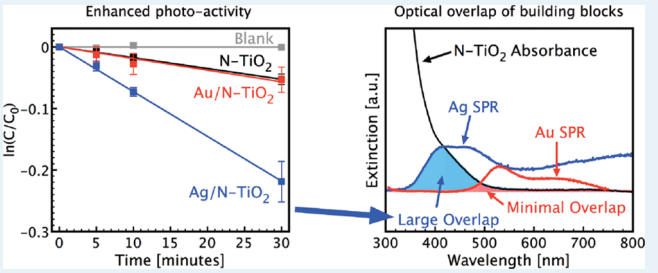

KEYWORDS: photocatalysis, plasmon enhancement, titanium dioxide, silver, predictive model

INTRODUCTION

A semiconductor photocatalyst absorbs photons with energy exceeding the material's band gap, transferring the energy of light into excited charge carriers (electron/hole pairs), which can then drive reactions at the photocatalyst surface. Oxide semiconductors have been shown to be useful for a range of photochemical transformations including photodecomposition of organics and water splitting.[1,2] However, due to low efficiencies of many abundant semiconductors in the conversion of incident photons to chemically useful charge carriers at the semiconductor surface, these photochemical processes often exhibit low rates.

It has been shown recently that photoexcited, plasmonic nanostructures of silver (Ag) embedded in a matrix of TiO_2 can enhance the photocatalytic activity of TiO_2.[3−6] The critical characteristic of the Ag/TiO_2 composites governing the enhancements in photocatalytic rates is high optical activity of Ag nanoparticles manifested in the light-induced excitation of surface plasmon resonance (SPR). It has also been shown that there are three primary mechanisms by which metal SPR can enhance the reaction rates on nearby semiconductors. In one mechanism, often termed the charge transfer mechanism, it is proposed that SPR leads to the transfer of charge carriers from photoexcited metal to the semiconductor, and that the energetic charge carriers induce photocatalytic transformations on the semiconductor.[7−10] Another mechanism is based on the interaction of the semiconductor with intense SPR-induced electromagnetic fields in the vicinity of the plasmonic nanostructure, leading to increased rates of e/h formation in the semiconductor.[3−6,11,12] This mechanism is often termed the near-field electromagnetic mechanism. The third mechanism is based on efficient scattering of resonant photons by plasmonic nanostructures, resulting in longer optical path lengths for photons in the semiconductor matrix that yields a higher rate of the formation of excited charge carriers. While it has been recognized that the photocatalytic reaction rates on the composite photocatalysts depend on multiple factors, including catalytic and optical properties of semiconductor and plasmonic metal building blocks and the geometric placement of the building blocks with respect to each other, the predictive models that capture the effects of these factors on the reaction rates are missing.

In this contribution we take a step toward developing these models by probing how the optical properties of individual building blocks affect the reaction rates on composite photocatalysts. Photocatalysts used in these studies were designed so that the dominant interaction between the building blocks was due to SPR-induced electromagnetic fields (i.e., the near-field electromagnetic mechanism). We show that the overlap between the wavelength of source photons, the absorption spectrum of the semiconductor, and the metal SPR spectrum is an excellent descriptor of photocatalytic activity of the composite photocatalysts. We arrived to these conclusions by testing the photocatalytic activity of two semiconductor photocatalysts with different optical properties, TiO_2 and nitrogen-doped TiO_2 (N-TiO_2), upon addition of two plasmonic metal nanostructures with different optical properties: nanocubes of Ag of ∼120 nm edge length and nanospheres of Au of ∼25 nm diameter. The use of two different semiconductors (TiO_2 and N-TiO_2), two different metals (Ag and Au) and different relative weight loadings of semiconductor and metal gives us sufficient flexibility to manipulate the optical properties of metal and semiconductors and correlate these to the photocatalytic activity of composite

Received: June 15, 2011
Revised: August 7, 2011
Published: September 12, 2011

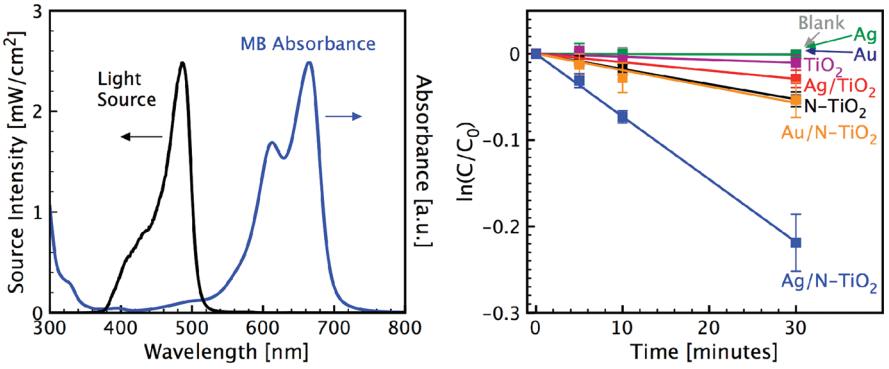

Figure 1. (a) Black curve: intensity of visible source with 500 nm short pass filter. Total intensity at the photocatalyst surface is 140 mW/cm^2. Blue curve: methylene blue absorption spectrum (arbitrary scale). (b) Aqueous phase MB decomposition over different photocatalysts: Ag cubes only (green), Au spheres only (dark blue), P25 TiO_2 only (purple), N-TiO_2 only (black), Ag/TiO_2 composite (red), Au/N-TiO_2 composite (orange) and Ag/N-TiO_2 (blue). The composite samples (Ag/TiO_2, Au/N-TiO_2, Ag/N-TiO_2) each contained 4.5% metal particles by weight. All semiconductor-only and composite samples contained constant weight of semiconductor particles. The uncatalyzed (blank) photolysis of MB showed immeasurable decomposition (gray points).

photocatalysts. The photocatalytic activity was quantified in studies of the photodecomposition of methylene blue (MB). MB is a bright blue organic dye molecule that is commonly used as an analog for water-soluble organic pollutants. MB is a strong absorber of light around 550−700 nm, so we have been careful to use a light source that does not overlap with the direct light absorbance of MB. We also demonstrate how this optical overlap descriptor of photocatalytic activity allows for rapid evaluation of potential effectiveness of plasmonic metal nanoparticles of particular composition, shape and size, as promoters of photochemical activity of random semiconductors with any light source.

METHODS

The TiO_2 photocatalyst was Degussa/Evonik P25 TiO_2 (∼20 nm diameter particles, ∼80% anatase phase). Nitrogen-doped TiO_2 (N-TiO_2) was synthesized by heating P25 TiO_2 particles in flowing gaseous NH_3 at 500 °C for 5 h, yielding N-TiO_2 powders with low N dopant concentrations. It has been shown previously that these N-TiO_2 photocatalysts show improved visible light activity compared to TiO_2.[13] Figure 2a shows extinction spectra for P25 TiO_2 and N-TiO_2, collected by tightly packing the powders into the sample cup of a Harrick diffuse reflectance cell and smoothing the surface. All spectra were collected with a ThermoScientific Evolution 300 spectrophotometer.

Cubic Ag nanoparticles were synthesized using a modified polyol process, described in detail in previous contributions.[14−16] Briefly, slow addition of $AgNO_3$ (precursor) and polyvinylpyrrolidone (stabilizer) to a solution of ethylene glycol (solvent and reductant) and dilute HCl (etchant) resulted in the formation of cubic Ag nanoparticles with a layer of polyvinylpyrrolidone (PVP) stabilizer on the surface. The particles were washed with acetone once via centrifugation and redispersed in 200-proof ethanol. The particle size (edge length of 118 ± 25 nm) was determined from scanning electron microscopy (SEM); a representative SEM image is shown in Figure 2b. Micrographs were obtained using an FEI Nova 200 Nanolab. The accelerating voltage was 5 kV. Spherical Au particles were synthesized in a process identical to that previously reported in detail for Ag nanospheres,[14] except that $AgNO_3$ is replaced with the same concentration of $AuCl_4$. The resulting Au spheres were 25.4 ± 4.5 nm in diameter, as measured by SEM (Figure 2c). The Au nanostructures were chosen for use in control experiments because their plasmon resonance is not excited by the filtered light source, as discussed below. We note that as used Ag and Au nanoparticles were coated with a nonconductive polymer layer (PVP); we comment more on this below.

Semiconductor (TiO_2 and N-TiO_2) and metal (Ag and Au) nanoparticles were independently suspended in pure ethanol and sonicated. Single-component samples (for example, TiO_2-only or Ag-only) were prepared by drop-coating these suspensions onto 1-cm^2 SiO_2 substrates and drying in a stagnant ambient atmosphere. Composite suspensions were prepared by combining the pure nanoparticle suspensions and thoroughly mixing using agitation and sonication. Composite photocatalyst samples (for example, Ag/TiO_2) were prepared by the same drop-coating method using the mixed nanoparticle suspensions, resulting in a physical mixture of the two types of particles on the substrate. UV−visible extinction spectra of the resulting samples are given in Figure 3a. All photocatalyst samples used in the experiments contained a constant 1 mg weight (as well as volume and surface area) of semiconductor particles. The amount of metal nanoparticles in the composite mixtures was varied. In the text and figures we report weight percent of the metal particles with respect to the constant weight of semiconductor particles.

To test the photochemical activity we measured the rate of photodecomposition of methylene blue (MB) under illumination with a broadband visible source. This process is activated by energetic holes at the semiconductor surface.[17,18] Reactions were carried out at room temperature in a liquid phase batch reaction vessel with an open top. Photocatalyst substrates were placed on the bottom of the vessel, 2 mL of 0.05 mM MB in water was added and the system was allowed to sit in the dark for 1 h prior to illumination. The system was continuously stirred and aerated by bubbling O_2. The reaction vessel was kept in a room temperature water bath to maintain isothermal reaction conditions.

The system was illuminated from the top by a visible light source with a wavelength range of ∼375−900 nm. MB demonstrates a strong absorbance of light from ∼550−700 nm (see Figure 1a); therefore, to prevent direct photolysis of MB we used a 500 nm short pass filter to cut off photons with wavelengths higher than 500 nm. This ensures that the reactant molecule is essentially transparent to the source photons,[19] also effectively preventing the possibility of dye sensitization. The total source power delivered to the catalyst surface was 140 mW/cm^2.

dx.doi.org/10.1021/cs200320h |ACS Catal. 2011, 1, 1441−1447

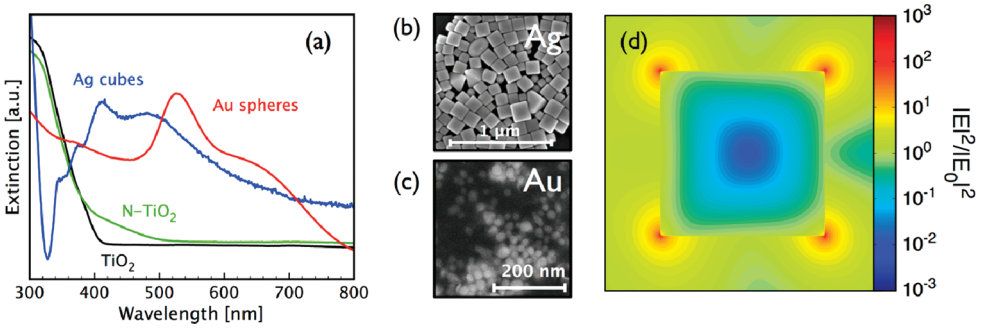

Figure 2. (a) Diffuse reflectance UV−visible (DRUV) spectra of TiO_2, N-TiO_2, Ag nanocubes and Au spheres. TiO_2 and N-TiO_2 samples were prepared by tightly packing the semiconductor powders into a sample cup and smoothing the top surface. Ag and Au samples were dried onto an SiO_2 substrate. (b) Scanning electron micrograph (SEM) of the Ag nanocube sample (edge length 118 ± 25 nm). (c) SEM of spherical gold particles (diameter 25.4 ± 4.5 nm). (d) Enhancement in electric field intensity at a wavelength of 450 nm (near the SPR peak) from an FDTD simulation of a 120-nm Ag cube in water.

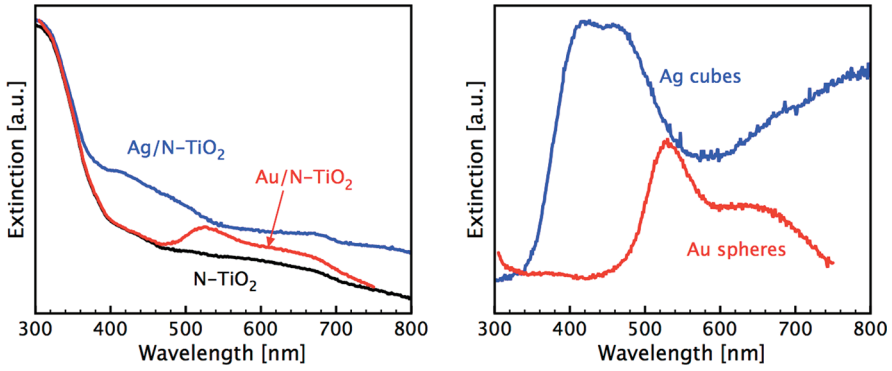

Figure 3. (a) Diffuse reflectance UV−visible (DRUV) spectra of N-TiO_2, Ag/N-TiO_2 composite (4.5 wt % Ag) and Au/N-TiO_2 composite (4.5 wt % Au) samples on SiO_2 substrates. See text for sample preparation. (b) Ag and Au difference spectra for the composite samples in Figure 2a, obtained by subtracting the N-TiO_2 spectrum from the composite spectra.

Figure 1a shows the wavelength distribution of the filtered source and the absorbance of MB. The MB concentration was monitored as a function of time by using transmission UV−visible spectroscopy to observe the decrease in the 610 nm MB peak.

Finite-difference time-domain (FDTD) optical simulations were performed to simulate the optical response of the materials as a function of the wavelength of incident photons. FDTD is a computational electro-dynamics modeling technique, which solves discretized Maxwell equations in space and time subject to the input geometry, material properties, and boundary conditions.[20] The optical properties of plasmonic metals were represented using a Drude-Lorentz model[21−23] with empirical optical constants,[24] which has been shown to give accurate results for Ag and Au nanostructures.[25,26] Water was used as the background dielectric medium. All simulations were periodic in the *x*- and *y*-directions, while the perfectly matched layer (PML) construct was used to truncate the simulations in the positive and negative *z*-directions. Incident radiation was supplied via a 300−800 nm Gaussian source. Scattering, absorbance and extinction cross sections were calculated using the total-field/scattered-field (TFSF) formalism.[20]

RESULTS AND DISCUSSION

Figure 1b shows the rate of MB decomposition over various catalysts using the broadband illumination source with 500 nm short pass filter. The figure shows that the illumination of the MB solution without photocatalysts showed no significant MB decomposition. The figure also shows that TiO_2 exhibited a fairly low MB decomposition rate. This low rate is the consequence of a relatively small overlap between the light source intensity extending to approximately 375 nm (Figure 1a) and the absorbance of TiO_2 extending to approximately 410 nm (Figure 2a). Figure 1b also shows that N-TiO_2 exhibits higher photocatalytic activity than TiO_2, which is not surprising since it absorbs over a broader range of the visible source spectrum than TiO_2. Furthermore, the figure shows that the addition of Ag nanocubes significantly enhanced the rate of MB decomposition over both TiO_2 and N-TiO_2. For example, the rate of MB decomposition on 4.5% Ag/N-TiO_2 was approximately 4 times larger than the rate on N-TiO_2. We observed that the addition of Au nanostructures has little effect on the reaction rate on TiO_2 and N-TiO_2.

To understand the results in Figure 1, we analyze the optical and catalytic properties of the building blocks used in the experiments. First, Figure 1b shows that Ag and Au nanostructures by themselves exhibit no photocatalytic activity under these operating conditions. Also, due to low doping with N, we can assume that the inherent capacity of TiO_2 and N-TiO_2 to support catalytic transformations by providing surface sites for reaction intermediates are very similar to each other. This essentially

dx.doi.org/10.1021/cs200320h |*ACS Catal.* 2011, 1, 1441–1447

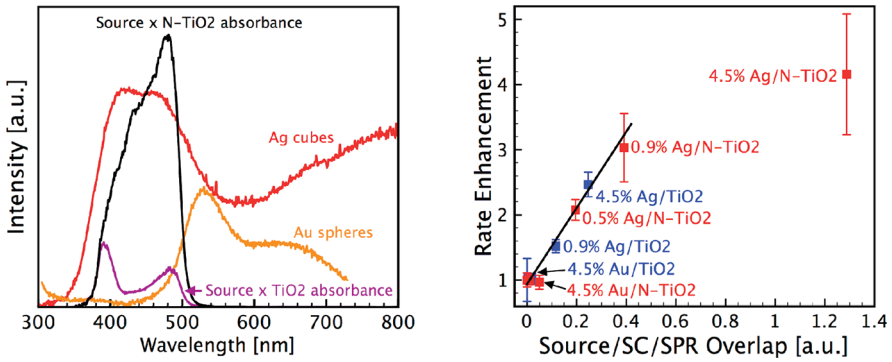

Figure 4. (a) Source/semiconductor absorbance overlap for N-TiO_2 (black curve) and TiO_2 (purple curve) and metal nanoparticle spectra (see Figure 3b) for 4.5% Ag and 4.5% Au. (b) Enhancement in the MB decomposition rate as a function of the overlap among illumination source, semiconductor absorbance and metal nanoparticle SPR. Blue points shows native TiO_2-based composites, and red points show N-TiO_2-based composites.

means it can be assumed that, in the limit of low dopant concentration,[13] the difference in the performance of composite materials is mainly a consequence of the difference in the optical properties of the building blocks contained in the composite photocatalysts rather than their inherent capacity to support chemical transformations.

The optical properties of the individual building blocks, measured as UV−vis extinction spectra, are shown in Figure 2a. The figure shows that the TiO_2 extinction drops dramatically at ∼380 nm and extends to 410 nm, whereas N-TiO_2 exhibits significant extinction intensity well into the visible region up to ∼500 nm. The extinction in semiconductors is the consequence of the absorption process, which results in the formation of excited charge carriers (e/h pairs). The formation of charge carriers is responsible for photocatalytic activity of both semiconductors. Figure 2a also shows that the main extinction feature of Ag nanocubes peaks at ∼450 nm whereas the Au spheres show maximum extinction at ∼600 nm. For both metals, the main extinction peaks are due to excitation of SPR. The extinction below the main spectral features (below ∼500 nm for Au and below ∼325 nm for Ag) is primarily due to interband transitions, which are not critical to the discussion herein. SPR can be described as the resonant photon induced oscillation of valence electrons, established when the frequency of photons matches the natural frequency of surface electrons oscillating against the restoring force of positive nuclei. SPR is characterized by intense oscillating electric fields that are a few orders of magnitude larger than the field associated with the source photons.[27] This is depicted in Figure 2d, which shows the calculated SPR-induced electric field enhancement from an FDTD simulation of a 120-nm Ag cube.

UV−vis extinction spectra for a few composite photocatalysts are shown in Figure 3. The figure shows that the composite extinction is a superposition of the extinction due to the individual semiconductor and metal building blocks in the composite. The fact that the composite systems exhibit this behavior is an indication that there is no significant light-induced charge transfer from one building block to another − charged semiconductor and plasmonic metals would exhibit additional extinction features.[7,28] This is not surprising, considering that the metal and semiconductor building blocks are separated by nonconductive organic molecules chemisorbed on the surface of metal nanostructures.

It has been shown previously for similar plasmonic metal/semiconductor composite systems that the metal SPR-induced enhancement in the photocatalytic activity of semiconductors, also depicted in Figure 1, is the consequence of the interaction of the SPR-induced intense oscillating electric field, concentrated around the metallic nanostructure (shown in in Figure 2d) and the nearby semiconductor.[3−6,11,12] Essentially, the SPR-induced electric field increases the rate of e/h formation in the semiconductor, which in turn results in higher reaction rates.

Below in this text we attempt to quantify the interaction of the metal SPR-induced electric field with the nearby semiconductor and in doing so relate the individual optical properties of metal and semiconductor building blocks to the photocatalytic activity of the composite photocatalysts. For a plasmonic metal to enhance the rate of e/h formation in the nearby semiconductor and therefore to increase the photocatalytic rates, the metal SPR−induced oscillating electric field must efficiently channel sufficient energy (i.e., the minimum energy required to overcome the band gap) into the nearby semiconductor. This essentially means that the there has to be an overlap between the metal SPR spectrum and the semiconductor absorption spectrum. Furthermore, since SPR is a resonant phenomenon, an excitation of SPR requires an overlap between the source spectrum and the metal SPR spectrum. This explains why the addition of Au does not enhance the activity of TiO_2 or N-TiO_2 in the composite photocatalysts that contained the Au nanostructures. As discussed above, the Au SPR is between ∼500 and 700 nm, and it is not excited by the filtered light source with intensity between 375 and 500 nm.

This analysis suggests a simple approximation that could relate the relative SPR-induced reaction rate enhancements on composite photocatalysts to the optical properties of individual building blocks. In this relationship, shown in eq 1, the reaction rate enhancement (r/r_0) is proportional to the optical overlap between the illumination source spectrum, the metal SPR (i.e., the extinction spectrum of the metallic building block), and the absorption spectrum of the semiconductor (illustrated in Figure 4a).

$$r/r_0 \propto \int I_0(\lambda)\, A_{SC}(\lambda)\, E_{SPR}(\lambda)\, d\lambda \qquad (1)$$

where I_0 is the wavelength-dependent source spectrum, A_{SC} is the semiconductor absorbance spectrum and E_{SPR} is the metal nanoparticle extinction arising from excitation of SPR. We comment on the general applicability of eq 1 with respect to the

dx.doi.org/10.1021/cs200320h |ACS Catal. 2011, 1, 1441−1447

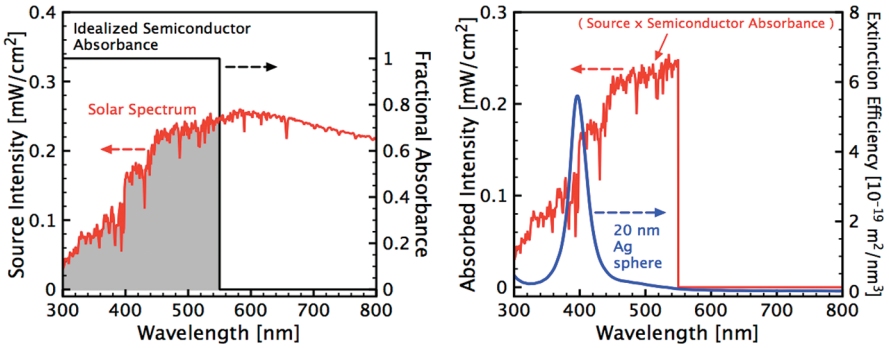

Figure 5. (a) Intensity of the solar spectrum (left ordinate) and fractional absorbance of an idealized SC with band gap of 550 nm (right ordinate). AM1.5 solar spectrum data are from NREL, http://rredc.nrel.gov/solar/spectra/am1.5/. The product of the two curves (shaded area) gives the number of photons absorbed by the SC as a function of wavelength. (b) Product of source intensity and SC absorbance, shown as the shaded area in Figure 6a (left ordinate), and simulated extinction (SPR) divided by particle volume for a 20-nm Ag sphere (right ordinate). Source/SC/SPR overlap is calculated by multiplying the two curves in Figure 6b and integrating from the metal interband transition wavelength (325 nm for Ag and 490 nm for Au) to 800 nm.

geometric arrangements of the individual building blocks further below in this text.

To test the relationship in eq 1, in Figure 4b, we plotted the MB photodecomposition rate enhancement as a function of the optical overlap among light source, semiconductor absorbance, and metal SP states for a range of tested photocatalysts. The rate enhancement is calculated as the measured MB decomposition rate (see Figure 1b) for a composite system divided by the rate for the semiconductor only (e.g., Ag/N-TiO_2 compared to N-TiO_2 and Ag/TiO_2 compared to TiO_2). The optical overlap was calculated, as shown in eq 1, by multiplying the illumination source spectrum (Figure 1a), the semiconductor absorbance spectrum (Figure 2a), and the metal nanoparticle extinction spectrum (Figure 3b) and integrating over the entire wavelength range (300−800 nm). The rate enhancement for a pure semiconductor is unity by definition, and the optical overlap for a pure semiconductor is defined as zero (since there are no SP states).

Figure 4 shows that for a given geometry of composite photocatalysts (with similar inherent catalytic activity), the optical overlap, as defined in eq 1, is linearly related to the measured rate enhancements for tested composite plasmonic metal/semiconductor photocatalysts. The exception to this is for high Ag loading, which significantly underperforms the otherwise linear trend. This is not surprising considering that high Ag loading results in high overall extinction of the composite photocatalyst, which can shift the overall process into a light-limited reaction regime, that is, the entire reactor volume is not exposed to light.

The relationship presented in eq 1 and validated experimentally in Figure 4 can be used to guide the design of composite photocatalysts. For example, the intensity and wavelength of metal SPR can be manipulated by changing the composition, shape, size or dieletric environment of metal nanoparticles.[29−31] Plasmonic nanoparticles of noble metals can be tuned to exhibit SPR spanning the entire near-UV/visible/near-IR spectrum.[32,33] It is beneficial to be able to identify, a priori, the plasmonic nanostructures that would yield the maximum enhancements in reaction rates on a given semiconductor. In this context, optical simulation techniques (e.g., the FDTD method) provide a very useful tool, since the optical properties of any arbitrary metal nanoparticle geometry can be calculated with reasonable accuracy using these simulations.

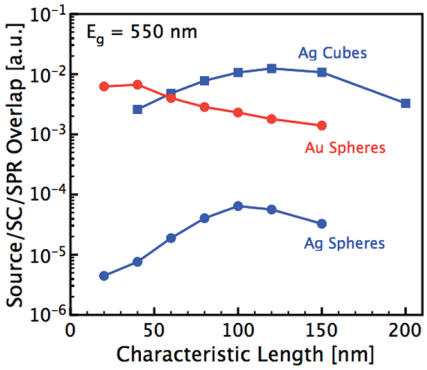

Figure 6. Calculated source/SC/SPR overlap integral as a function of the characteristic length (diameter for spheres and edge length for cubes) of plasmonic nanoparticles for an idealized SC with a band gap of 550 nm. The light source was the AM1.5 solar spectrum (data from the NREL, http://rredc.nrel.gov/solar/spectra/am1.5/).

We have used the model in eq 1 to probe the effect of metal particle size, shape, and composition on the photochemical activity of a model semiconductor that absorbs light with wavelengths below 550 nm. In these studies, the absorbance of a semiconductor was modeled using a step function with full absorbance below 550 nm and no absorbance above 550 nm (see Figure 5a). The metal SPR spectra were evaluated by calculating the extinction normalized by particle volume using the FDTD optical simulations. This normalization allows for a comparison of the effectiveness of different shape and sizes of nanoparticles on a mass basis. The illumination source spectrum for these calculations was the AM1.5 solar spectrum (National Renewable Energy Laboratory (NREL), Golden, Colorado; http://rredc.nrel.gov/solar/spectra/am1.5/). The optical overlap, which is proportional to the reaction rate enhancement, was evaluated as in eq 1. The lower limit of integration was the wavelength below which interband transitions, rather than SPR, dominate the metal extinction spectra (325 nm for Ag and 490 nm for Au);[32] the upper limit was 800 nm.

Figure 6 shows the calculated optical overlap as a function of particle size (sphere diameter or cube edge length) for three different plasmonic nanoparticles: Ag spheres, Ag cubes, and Au

dx.doi.org/10.1021/cs200320h |ACS Catal. 2011, 1, 1441–1447

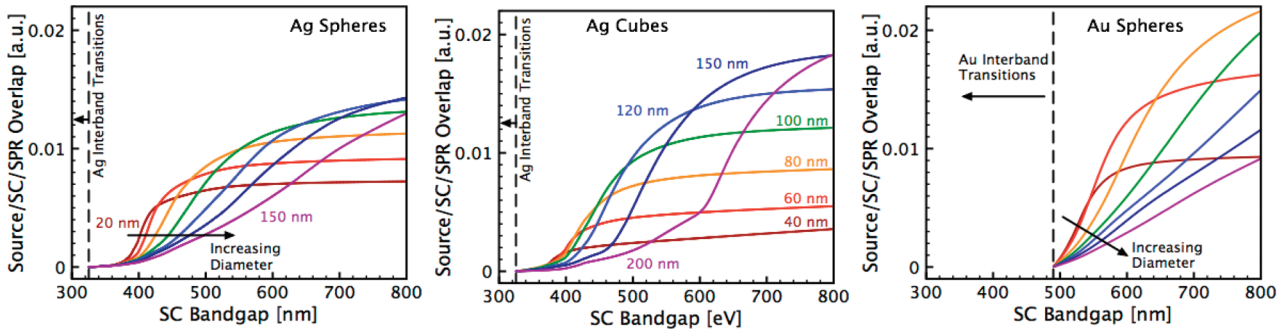

Figure 7. Calculated source/SC/SPR overlap integral as a function of semiconductor (SC) band gap. Illumination source was the AM1.5 solar spectrum (data from the NREL, http://rredc.nrel.gov/solar/spectra/am1.5/) for (a) Ag spheres with varying diameters, (b) Ag cubes with varying edge length, and (c) Au spheres with varying diameters. Cube edge lengths are labeled in part b. Sphere diameters in parts a and c are 20, 40, 60, 80 100, 120, and 150 nm. The overlap quantity is not calculated at wavelengths lower than the metal interband transition (~325 nm for Ag and ~490 nm for Au).

spheres. In general, large Ag cubes (edge length ~120 nm) and smaller Au spheres (edge length 50 nm) have the highest overlap with the 550 nm band gap semiconductor under solar illumination. We anticipate that these plasmonic nanostructures should show the highest photocatalytic rate enhancement. Figure 6 also indicates that for a 550 nm band gap semiconductor under solar illumination, Au spheres should out-perform Ag spheres for a broad range of sizes. This is primarily due to the difference in SPR wavelengths for Ag and Au. For small spheres, the Ag SPR is centered around 390 nm, where the solar illumination has a relatively low intensity (see Figure 5), whereas the Au SPR is centered around 550 nm, where the illumination is much more intense. Ag cubes generally out-perform Au spheres primarily because, for a given particle size and composition, cubic nanoparticles intrinsically have a much larger extinction efficiency.[4] In addition, the spectra for cubes are generally broader than for spheres, which increases overlap.

Although Figure 6 specifically focuses on a semiconductor with 550 nm band gap under solar illumination, the method we have detailed allows extension to any semiconductor and light source. For example, by simply changing the band gap of our idealized semiconductor from 550 nm to any value, we can determine which metal nanostructures are promising for any given semiconductor band gap under solar illumination. The results of this analysis are shown in Figure 7a (Ag spheres), b (Ag cubes), and c (Au spheres), which display the calculated optical overlap for a given metal particle (composition, shape, and size) as a function of the semiconductor band gap.

Figure 7 shows that for semiconductors with a large band gap (~3 eV), small Ag nanostructures exhibit the highest overlap integral and should lead to the largest enhancements in reactions rates. The main reason for this is a relatively high intensity of SPR of these Ag nanostructures under UV light. For semiconductors with a small band gap, fairly large Ag and smaller Au nanostructures show the most promise. Although we have focused on three specific metal nanoparticle examples, the model is easily extended to any metal composition, shape, and size with the only necessary input being the inclusion of the appropriate bulk metal optical properties in the FDTD simulations (i.e., the complex dielectric function that can be fit using, for example, a Drude-Lorentz model).[23]

The optical overlap integral in eq 1 represents a simple predictor allowing us to compare the performance of semiconductor/plasmonic metal composite photocatalysts based only on the far-field optical properties of the building blocks (extinction spectra). As noted above, the analysis assumes that the difference in performance is a consequence of the optical properties of the building blocks within the composites. This assumption was reasonable for comparing TiO_2 and N-TiO_2 due to the low level of N doping, but differences may arise if high levels of doping are used, since this can actually decrease photoactivity while increasing extinction.[13] Equation 1 also assumes that the interaction between the composite building blocks can be captured by the far-field extinction spectra.

The model systems used herein are characterized by closely spaced (<20 nm spacing) semiconductor and metal building blocks. As stated above, we have established previously for these systems that the near-field electromagnetic mechanism dominates the interaction between the building blocks. Therefore, the applicability of eq 1 depends on the extent to which the far-field extinction spectra due to metal SPR can capture the near-field, SPR-induced electromagnetic fields in the neighborhood of the plasmonic metallic nanostructure. To make this a reasonable assumption and address the fact that the electromagnetic fields are not homogeneous around a plasmonic nanostructure, the use of the far-field spectra in eq 1 to compare the performance of different composite photocatalysts requires a similar geometric arrangement of the metal and semiconductor building blocks,[34,35] that is, there should be a consistent spatial overlap between the SPR-induced electric fields and the semiconductor particles among different composite photocatalysts. Finally, we also note that eq 1 applies for comparing the performance of composite photocatalysts, for which the rate of parasitic loss of e/h due to the presence of the metal surface is constant.

CONCLUSIONS

We demonstrated the design of a composite plasmonic metal/semiconductor photocatalysts that show enhanced photocatalytic activity compared with the semiconductor alone. The observed photocatalytic activity enhancement is attributed to metal SPR, which can increase the rate of formation of charge carriers within the semiconductor. We showed that the optical overlap among the illumination source spectrum, semiconductor absorbance spectrum, and metal nanoparticle SPR spectrum provides a useful descriptor for predicting the SP-induced rate enhancement for composite photocatalysts of similar geometries (specifically, similar arrangements of the nanosized building blocks) and guiding the formulation of optimal plasmonic metal/semiconductor photocatalysts.

AUTHOR INFORMATION

Corresponding Author
*E-mail: linic@umich.edu.

ACKNOWLEDGMENT

We gratefully acknowledge support from the U.S. Department of Energy, Office of Basic Energy Sciences (FG-02-05ER15686) and the NSF, Division of Chemistry (1111770). S.L. also acknowledges a DuPont Young Professor grant and a Camille Dreyfus Teacher-Scholar Award from the Camille & Henry Dreyfus Foundation.

REFERENCES

(1) Linsebigler, A. L.; Lu, G.; Yates, J. T., Jr. *Chem. Rev.* **1995**, *95*, 735.
(2) Fujishima, A.; Zhang, X.; Tryk, D. A. *Surf. Sci. Rep.* **2008**, *63*, 515.
(3) Awazu, K.; Fujimake, M.; Rockstuhl, C.; Tominaga, J.; Murakami, H.; Ohki, Y.; Yoshida, N.; Watanabe, T. *J. Am. Chem. Soc.* **2008**, *130*, 1676.
(4) Christopher, P.; Ingram, D. B.; Linic, S. *J. Phys. Chem. C* **2010**, *19*, 9173.
(5) Kumar, M. K.; Krishnamoorthy, S.; Tan, L. K.; Chiam, S. Y.; Tripathy, S.; Gao, H. *ACS Catal.* **2011**, *1*, 300.
(6) Ingram, D. B.; Linic, S. *J. Am. Chem. Soc.* **2011**, *133*, 5202.
(7) Tian, Y.; Tatsuma, T. *J. Am. Chem. Soc.* **2005**, *127*, 7632.
(8) Kowalska, E.; Mahaney, O. O. P.; Abe, R.; Ohtani, B. *Phys. Chem. Chem. Phys.* **2010**, *12*, 2344.
(9) Primo, A.; Corma, A.; García, H. *Phys. Chem. Chem. Phys.* **2011**, *13*, 886.
(10) Tian, Y.; Tatsuma, T. *Chem. Commun.* **2004**, 1810.
(11) Liu, Z.; Hou, W.; Pavaskar, P.; Aykol, M.; Cronin, S. B. *Nano Lett.* **2011**, *11*, 1111.
(12) Hou, W.; Liu, Z.; Pavaskar, P.; Hung, W. H.; Cronin, S. B. *J. Catal.* **2011**, *277*, 149.
(13) Irie, H.; Watanabe, Y.; Hashimoto, K. *J. Phys. Chem. B* **2003**, *107*, 5483.
(14) Christopher, P.; Linic, S. *ChemCatChem* **2010**, *2*, 78.
(15) Christopher, P.; Xin, H.; Linic, S. *Nat. Chem.* **2011**, *3*, 467.
(16) Im, S. H.; Lee, Y. T.; Wiley, B.; Xia, Y. *Angew. Chem., Int. Ed.* **2005**, *44*, 2154.
(17) Mills, A.; Wang, J. *J. Photochem. Photobiol., A* **1999**, *127*, 123–134.
(18) Houas, A.; Lachheb, H.; Ksibi, M.; Elaloui, E.; Guillard, C.; Herrmann, J.-M. *Appl. Catal., B* **2001**, *31*, 145–157.
(19) Yan, X.; Ohno, T.; Nishijima, K.; Abe, R.; Ohtani, B. *Chem. Phys. Lett.* **2006**, *429*, 606.
(20) Taflove, A.; Hagness, S. C. *Computational Electrodynamics: The Finite-Difference Time-Domain Method*; Artech House: Boston, 2005.
(21) Wooten, F. *Optical Properties of Solids*; Academic Press: New York, 1972.
(22) Ashcroft, N. W.; Mermin, N. D. *Solid State Physics*; Holt, Rinehart and Winston: New York, 1976.
(23) Lee, T.-W.; Gray, S. K. *Opt. Express* **2005**, *13*, 9652.
(24) Palik, E. D. *Handbook of Optical Constants of Solids*; Academic Press: New York, 1985.
(25) Link, S.; El-Sayed, M. A. *J. Phys. Chem. B* **1999**, *103*, 8410.
(26) McMahon, J. M.; Wang, J.; Sherry, L. J.; Van Duyne, R. P.; Marks, L. D.; Gray, S. K.; Schatz, G. C. *J. Phys. Chem. C* **2009**, *113*, 2731.
(27) Brus, L. *Acc. Chem. Res.* **2008**, *41*, 1742.
(28) Kamat, P. V. *J. Phys. Chem. B* **2002**, *106*, 7729.
(29) Burda, C.; Chen, X.; Narayanan, R.; El-Sayed, M. A. *Chem. Rev.* **2005**, *105*, 1025.
(30) Kelly, K. L.; Coronado, E.; Zhao, L. L.; Schatz, G. C. *J. Phys. Chem. B* **2003**, *107*, 668.
(31) Linic, S.; Christopher, P. *ChemCatChem* **2010**, *2*, 1061.
(32) Rycenga, M.; Cobley, C. M.; Zeng, J.; Li, W.; Moran, C. H.; Zhang, Q.; Qin, D.; Xia, Y. *Chem. Rev.* **2011**, DOI: 10.1021/cr100275d.
(33) Xia, Y.; Xiong, Y.; Lim, B.; Skrabalak, S. E. *Angew. Chem., Int. Ed.* **2009**, *48*, 60.
(34) Maier, S. A.; Brongersma, M. L.; Kik, P. G.; Atwater, H. A. *Phys. Rev. B* **2002**, *65*, 193408.
(35) Ross, B. M.; Lee, L. P. *Opt. Lett.* **2009**, *34*, 896.

NOTE ADDED AFTER ASAP PUBLICATION

After this paper was published online September 23, 2001, a correction was made to eq 1. The corrected version was published October 7, 2011.